# Anchoring Screening of Defects Interaction in a Nematic Liquid Crystal

A. Bogi,[1] P. Martinot-Lagarde,[2] I. Dozov,[3] and M. Nobili[1]

[1]*Groupe de Dynamique des Phases Condensées, CNRS–Université Montpellier II, Place E. Bataillon, 34090 Montpellier, France*
[2]*Laboratoire de Physique des Solides, Bâtiment 510, Université Paris-Sud, 91405 Orsay Cedex, France*
[3]*Nemoptic LCD Advanced Tecnology, 1, rue Guynemer, 78114 Magny les Hameaux, France*

(Received 24 March 2002; published 7 November 2002)

The relaxation dynamic of a dipole of $+1/2$ and $-1/2$ parallel disclination lines in a confined geometry is measured. The confinement and the planar anchoring conditions force the disclinations to be normal to the glass plates. In a first asymptotic regime, the direct elastic interaction between disclination is completely screened out by the anchoring energy. In a second regime, corresponding to the final annihilation steps, the dynamic follows the square-root law predicted by de Gennes for two isolated and parallel disclinations. The annihilation dynamic, in the asymptotic regime, is in good agreement with an elastic model based on an electrostatic analogy.

DOI: 10.1103/PhysRevLett.89.225501 PACS numbers: 61.30.Jf, 47.35.+i, 61.30.Hn

Defects in nematic liquid crystal are topological objects related to a discontinuity of the director field **n(r)**, where **n(r)** is the average orientation of the elongated molecules composing the nematic medium. The topological properties of these defects have been broadly studied [1]. For isolated line defects (disclinations), the static (i.e., elastic energy and the force between disclinations) and dynamical properties are also well understood [2–4]. In real systems, disclinations are never isolated, being subjected to the anchoring forces coming from the substrates of the cell containing the liquid crystal. As a consequence, in a confined geometry, the substrate anchoring is expected to strongly influence the interactions between defect lines. A similar anchoring effect has been recently invoked to explain the annihilation dynamic of nematic point defects confined in capillary tubes [5] and in hybrid cells [6,7]. However, the behavior of defect lines in a confined geometry remains totally unexplored.

The study of topological defects is a highly interdisciplinar field in physics. The dynamics and the interaction of topological defects plays an important role in the understanding of defects mediated phase transitions, dissipation process in superfluid and superconductor, etc., Moreover, a confined geometry has dramatic effects on defects interaction as has been recently recognized in the case of vortex lines in extremely anisotropic layered superconductors [8,9], and in vortices trapped in superfluid Fermi gases [10].

The nematic liquid crystals are a convenient system to study the confinement effects on defects interactions. First, the disclinations appear spontaneously at the isotropic-nematic transition when the $O(3)$ symmetry of the isotropic phase is broken to the $D_{\infty h}$ symmetry of the nematic phase. Second, nematic defects are macroscopic objects which can be simply studied with an optical polarizing microscope. Third, a highly confined system can be easily obtained by approaching the solid substrates limiting the nematic.

In this Letter, we study the relaxation dynamic of a dipole of $+1/2$ and $-1/2$ disclination lines in a confined geometry. Because of the confinement and to the planar anchoring conditions the disclinations are normal to the glass plates. We measure two different dynamic regimes depending on the distance $u$ between the defect lines. When $u \gg \xi_0$, where $\xi_0$ is a characteristic length, the direct elastic interaction between disclination is completely screened out by the anchoring energy. The elastic force in this asymptotic regime has been calculated from an analogy with the electrostatic. In the second regime, corresponding to $u < \xi_0$, the annihilation dynamic follows the square-root law predicted by de Gennes [11] for two isolated and parallel disclinations.

In the experimental setup, the nematic liquid crystal 5CB (pentylcyanobiphenyl) is sandwiched between a planar glass plate and a convex spherical lens of bending radius $R = 52$ cm. The lens is mounted on a holder provided of three screws-springs systems to adjust the lens-plate distance up to 100 $\mu$m. All measurements have been done in the thinner cell region $r = 0$ where the thickness gradient is negligible. A 300 Å SiO layer is evaporated at 60° incident angle on the substrates to give a planar homogeneous anchoring. The easy axes on the two substrates are parallel, resulting in a uniform director orientation across the cell. The sample is placed in an oven (INSTEC STC200D) kept at $\Delta T = 0.2\,^{\circ}$C below the nematic clearing temperature. Under a polarizing microscope, the ordinary-extraordinary ray interference results in concentric rings due to the light optical path difference $\delta(r) = \Delta n d(r)$ [$\Delta n$ is the liquid crystal birefringence and $d(r)$ is the cell thickness]. $d(r = 0)$ can be adjusted with 1 $\mu$m steps by measuring the interference fringe order in white and in monochromatic light. A short pulse of hot air is injected into the oven to heat the liquid crystal in the isotropic phase. Shortly after the pulse, the sample temperature decreases to the oven temperature and the nematic phase is restored. The time $\tau$ necessary to the

  

sample for reaching the equilibrium temperature in the nematic phase has been measured by monitoring the interference rings shift induced by the quench. We found $\tau \approx 1$ s in agreement with a thermal diffusion time across the glass plates $\tau_D = h^2/D = 1.5$ s ($h = 1$ mm is the glass plate thickness and $D = 0.6 \times 10^{-6}$ m$^2$/s is the glass thermal diffusion coefficient). The experiment is filmed with a CCD camera connected to a PC. This system is able to store 33 image/s on the PC.

The transition from the high symmetry isotropic phase [$O(3)$] to the lower symmetry nematic phase ($D_{\infty h}$) generates topological line defects (disclinations). Figure 1 shows typical disclinations under crossed polarizers for a cell thickness $d = 13$ $\mu$m. Each defect has two extinction branches characteristic of a $\pm 1/2$ disclination. To preserve the null topological charge of the uniformly oriented nematic cell, the disclinations appear in $(-1/2)$-$(+1/2)$ pairs. The confinement and the planar anchoring condition force the wedge disclinations to be orthogonal to the substrates. Consequently, the director field lies in planes parallel to the substrate. The elastic distortion is confined in the region between the two disclinations. We call $\phi$ the director angle with the $y$ axis in Fig. 1. The $\phi$ field is mapped by turning the polarizers with respect to the cell. Far from the disclinations, $\mathbf{n}$ is uniformly oriented along the anchoring easy axis $\phi = \phi_0 = 0$. By approaching the defect dipole along the $y$ axis ($y > 0$) the director orientation moves toward the $x$ axis parallel to the line connecting the defects. By crossing the $x$ axis, $\mathbf{n}$ jumps from $\phi = \pi/2$ to $\phi = -\pi/2$ due to the defects topological charge. Finally, moving off from the dipole, the director recovers an orientation parallel to the anchoring easy axis direction. From an elastic point of view, this director distortion is equivalent to a continuous $\pi$ wall. The distance $\xi(t)$ along the $y$ axis between the extinction branches is a typical wall distortion length. During the defects annihilation, when the two disclinations are far apart, as in Figs. 1(a) and 1(b), $\xi(t) = \xi_0 \approx 5$ $\mu$m, independent from the distance between defects $u$. At the opposite, when $u(t) \leq \xi_0$ [see Figs. 1(c) and 1(d)], the extinction branches assume a circular form corresponding to $\xi(t) = u(t)$. These two different regimes are also found in the disclination annihilation dynamic in Fig. 2. The time origin is kept at $3\tau \approx$ 3s after the quench in the nematic phase guaranteeing a stable sample temperature during the dipole annihilation. For $u > \xi_0$, the disclinations relax with a constant speed, while, for $u < \xi_0$, the distance between defects follows a square-root time law.

In the asymptotic regime ($u \gg \xi_0$), the annihilation driving force is $F_0' = -d\mathcal{F}_{\text{exc}}/du$, where $\mathcal{F}_{\text{exc}}$ is the free elastic energy excess in the wall between the two defects. By using the axis definition shown in Fig. 1, we define normalized coordinates $y = \sqrt{K_2/K}\frac{\pi}{\ell}y'$ and $z = \frac{\pi}{\ell}z'$, where $K_2$ and $K$ are, respectively, the twist and splay-bend elastic constants and $\ell$ is a characteristic length given in (5) . The normalized force $F_0 = 2F_0'/\sqrt{K_2 K}$ writes as

$$F_0 = \int\left[\left(\frac{d\phi}{dz}\right)^2 + \left(\frac{d\phi}{dy}\right)^2\right]dydz + \frac{\ell}{L\pi}\int \sin^2\phi_S dy, \quad (1)$$

where $\phi_S$ is the surface director angle with the $y$ axis and $L$ is the anchoring extrapolation length. The first term in (1) is the bulk elastic energy; the second represents the Rapini-Papoular anchoring energy. By assuming a symmetrical cell with identical substrates, $\phi(y, z)$ can be found by minimizing the functional $F_0$ (1) in only half of the cell. The minimization gives

$$\frac{\partial^2\phi}{\partial y^2} + \frac{\partial^2\phi}{\partial z^2} = 0, \quad (2)$$

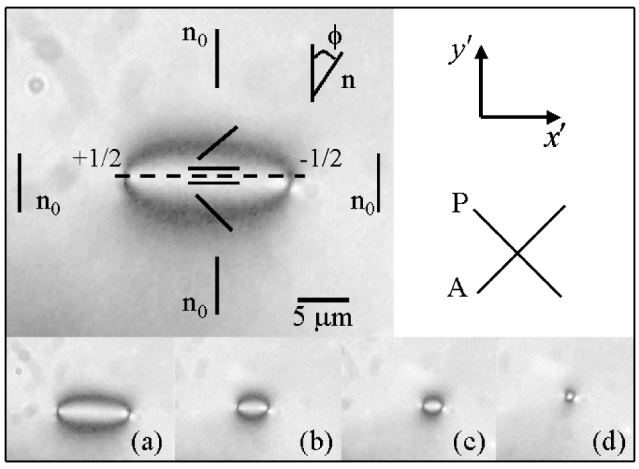


FIG. 1. $+1/2$ and $-1/2$ parallel disclination pair with the associated director texture. Disclination annihilation: (a) $t =$ 1.5 s; (b) $t = 1.75$ s; (c) $t = 1.78$ s; and (d) $t = 1.82$ s.

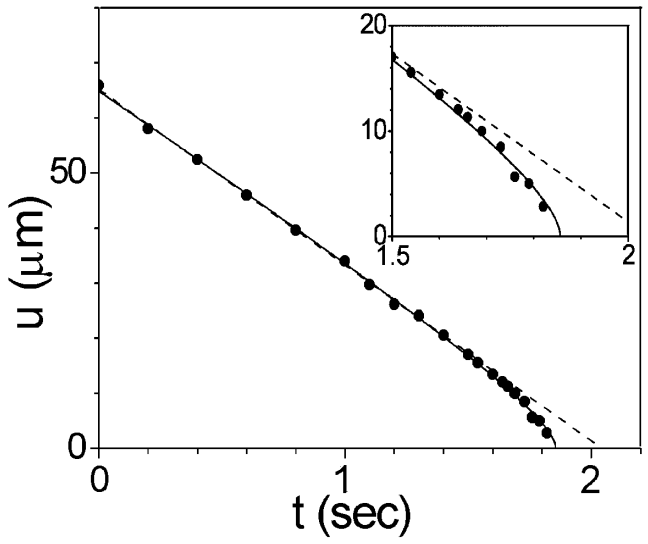


FIG. 2. Dipole annihilation dynamic. • are experimental points. The full line is the best fit with function (12). The dashed line is the extrapolation with a constant speed $v_{\text{asy}}$.

with boundary conditions

$$\left.\frac{\partial\phi}{\partial z}\right|_{z=(\pi/2)-(\pi d/2\ell)} = \frac{\ell}{2L\pi}\sin(2\phi_S),$$

$$\left.\frac{\partial\phi}{\partial z}\right|_{z=(\pi/2)} = 0, \tag{3}$$

$$\left.\frac{\partial\phi}{\partial y}\right|_{y=\pm\infty} = 0; \tag{4}$$

$\phi(y,z)$ obey to the Laplace equation with Neumann boundary conditions. To solve (2) and (3), we use the conformal transformation technique already developed in electrostatic. The detailed calculations will be reported elsewhere. The equilibrium distortion $\phi(y,z)$ in the wall is equivalent to a distortion associated with two virtual twist disclinations parallel to substrates, as in Fig. 3. Each virtual disclination is at a distance $z_0 = \arctan(L\pi/\ell)$ from the substrate where $\ell$ is found from the implicit equation

$$\ell\left[1 - \frac{2}{\pi}\arctan\left(\frac{L\pi}{\ell}\right)\right] = d. \tag{5}$$

The equilibrium director angle across the wall $\phi(y,z)$ is given by

$$\phi(y,z) = \frac{1}{2}\arctan\left(\frac{2\sinh y \sin z}{\sinh^2 y - \sin^2 z}\right). \tag{6}$$

In the case of weak anchoring $\ell = \pi\sqrt{(Ld)/2} \gg d$ and $\phi(y,z)$, (6) is found independent from $z$. In this limit, the bulk twist elastic torque overcomes the anchoring energy torque. As a consequence, the surface director moves toward the bulk director orientation to minimize the twist elastic energy. The distortion along the wall is a pure splay-bend distortion without twist. In the opposite limit of strong anchoring ($L \ll d$), $\ell \approx d$, and the anchoring torque is sufficiently strong to support a bulk twist distortion.

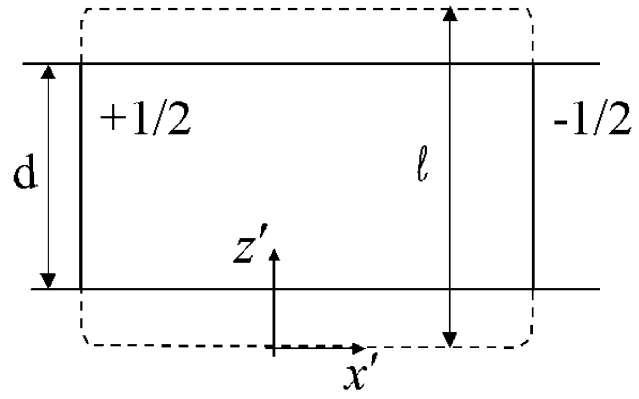


FIG. 3. Virtual disclinations placed at a distance $z_0' = (\ell/\pi)\arctan(L\pi/\ell)$ from the substrate.

The driving force $F_0$ is obtained by integrating Eq. (1) with the equilibrium director angle $\phi(y,z)$ given by Eq. (6):

$$F_0 = 2\sqrt{KK_2}\left[\frac{\pi}{2} - \arctan\left(\frac{L\pi}{\ell}\right) + \int_0^1 \frac{1}{t}\arctan\left(\frac{\ell}{L\pi}t\right)dt\right]. \tag{7}$$

The first two terms in (7) come from the anchoring energy, whereas the last term represents the bulk elastic energy. We limit here to discuss the strong anchoring conditions $L \ll d$. In this limit the leading terms in $F_0$ write as

$$F_0 = 2\sqrt{KK_2}\left[\frac{\pi}{2} - 1 + C + \frac{\pi}{2}\ln\left(\frac{d}{\pi L}\right)\right], \tag{8}$$

where $C = \int_0^1 \arctan(x)/x\,dx = 0.916$ is the Catalan number. The direct elastic interaction between defects gives an elastic force $F_e = (\pi K d)/(2u)$ [11]. The total elastic force $F_T$ acting on one disclination may be written in an approximate way by adding the two asymptotic forces $F_0$ and $F_e$. We obtain $F_T = F_0(1 + \xi_c/u)$, where $\xi_c = (\pi K d)/(2F_0)$. In the asymptotic regime $u \gg \xi_c$, the direct elastic interaction between defects is completely screened out by the anchoring. At the opposite, when the defects are closer than $\xi_c$, we recover the elastic interaction of two anchoring-free disclinations. Therefore $\xi_c$ represents the radius of a cylinder around each defect where the elastic torque associated to the defects dominates the anchoring torque.

The defects dissipate energy during their motion. The energy dissipation is confined in the cylinder of radius $\xi_c$ around the defects where the director changes rapidly in time. By neglecting the disclination core dissipation, the associated viscous force $F_v$ on each defect writes as [4]

$$F_v = \frac{\pi}{4}\gamma_{\text{eff}} d v \ln\left(3.6\frac{\xi_c}{a}\right). \tag{9}$$

In (9), $a$ is the disclination core radius, $v$ is the defect velocity, $\gamma_{\text{eff}}$ is an effective viscosity which takes into account backflow effects. Following [3], we can estimate $\gamma_{\text{eff}} = \gamma_1 - \alpha_2^2/[2(\eta_b - \gamma_2)]$, where $\gamma_1$ is the orientational viscosity and $\alpha_2$, $\eta_b$, $\gamma_2$ are related to the Leslie coefficients. $\gamma_{\text{eff}}$, in principle, has to be determined by solving the full equation of nematodynamic, therefore the above estimation of $\gamma_{\text{eff}}$ has to be considered correct to 20%.

The relative equation of motion of the two disclinations results in

$$\frac{du}{dt} = -v_{\text{asy}}\left(1 + \frac{\xi_c}{u}\right), \tag{10}$$

where

$$v_{\text{asy}} = \frac{8F_0}{d\pi\gamma_{\text{eff}}\ln(\frac{3.6\xi_c}{a})} \tag{11}$$

is the initial annihilation speed after the quench in the nematic phase. Equation (10) has an implicit solution:

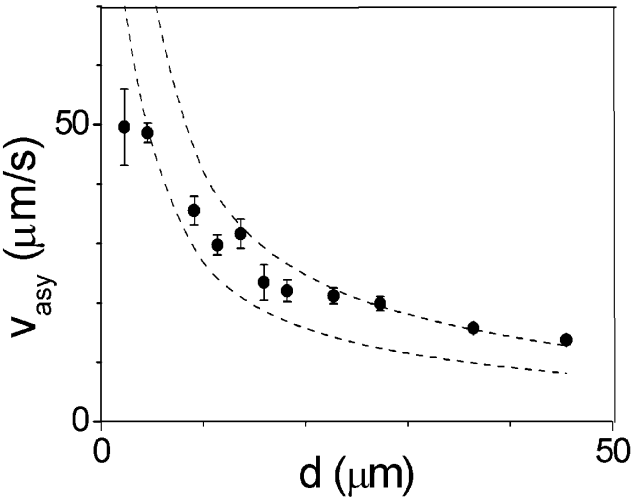


FIG. 4. $v_{asy}$ versus $d$. Dashed curves correspond to a plot with function (13) with $A = 70\ s^{-1}$ and $A = 110\ s^{-1}$, respectively.

$$v_{asy}t = u_0 - u - \xi_c \ln\left(\frac{u + \xi_c}{u_0 + \xi_c}\right). \tag{12}$$

$u_0$ in (12) is the initial distance between disclinations. The full line in Fig. 2 is the best fit of the experimental data with two free parameters $v_{asy}$ and $\xi_c$. We found $\xi_c \approx \xi_0 \approx 3.9\ \mu$m. The size $\xi_c$ of the region where the energy is dissipated is much larger than the core disclination radius supporting the assumption of a negligible core dissipation in (9). $L$ may be deduced from the $\xi_c$ and $v_{asy}$ best fit values. $\xi_c$ depends on the exact form of the total force in the region where the $F_0$ and $F_e$ are of the same order which is not well known. As a consequence, the $L$ determination from $\xi_c$ is less accurate than from $v_{asy}$. Using (11), from the best fit value $v_{asy} = 29\ \mu$m/s and the 5CB material parameters, $K = 2.4 \times 10^{-12}N$, $K_2 = 10^{-12}N$ [12], $a = 100$ Å, $\gamma_{eff} = 1.8$cp [13], we found $L = 0.2\ \mu$m. The anchoring extrapolation length is in agreement with the measured values for planar SiO anchoring [14]. To test our model in a closer way, we measure $v_{asy}$ versus $d$ (see Fig. 4). From (8) and (11), $v_{asy}$ is written as

$$v_{asy} \approx \frac{A}{d}\left[1 + \ln\left(\frac{d}{\pi L}\right)\right], \tag{13}$$

where $A = 8\sqrt{KK_2}/[\gamma_{eff} \ln(3.6\xi_c/a)] = 90 \pm 20\ s^{-1}$. The two dotted lines in Fig. 4 represent the plot of the function (13) with the two extrema $A$ values $A = 70\ s^{-1}$ and $A = 110\ s^{-1}$, respectively. From Fig. 4, one can see that experimental data support our anchoring screening model of disclinations interaction.

We summarize by stressing that a more stringent comparison with the theory requires a closer examination of the viscous force acting on the defects. In particular, the backflow effects, which have been taken into account in our model as the average of pure splay and bend viscosities, has to be calculated in a more detailed way starting from the full hydrodynamic equation for the two-dimensional flow around the defect. A second contribution to the viscous force may come from the surface static friction induced by the SiO surface roughness. This contribution is negligible in our case of strong driving force (strong anchoring) but it may become important in the weak elastic force limit (weak anchoring).

Very recently Tóth *et al.* [15] showed (through a numerical calculation) that the annihilation velocity for two parallel and isolated line defects depends on the topological charge of the defects. Our system, implemented with memory free surfaces having completely degenerate azimuthal anchoring and strong zenithal anchoring, is well suitable to an experimental test of their theoretical previsions.

In conclusion, we have studied the anchoring influence on the annihilation dynamic of two parallel $+1/2$, $-1/2$ disclination lines in a nematic liquid crystal. When the defect lines are far from each other, the direct elastic interaction is completely screened out by the anchoring energy. From the annihilation dynamic measurements, by using an elastic model based on an electrostatic analogy, we are able to find the anchoring strength.

We acknowledge fruitful discussions with S. Faetti.

[1] M. Kleman, Rep. Prog. Phys. **52**, 555 (1989).
[2] S. Chandrasekhar and G. S. Ranganath, Adv. Phys. **35**, 507 (1986).
[3] P. E. Cladis, W. van Saarloos, P. L. Finn, and A. R. Kortan, Phys. Rev. Lett. **58**, 222 (1987).
[4] G. Ryskin and M. Kremenetsky, Phys. Rev. Lett. **67**, 1574 (1991).
[5] G. G. Peroli and E. G. Virga, Phys. Rev. E **59**, 3027 (1999).
[6] O. D. Lavrentovich and S. Rozhkov, JETP Lett. **47**, 254 (1988).
[7] K. Minoura, Y. Kimura, K. Ito, and R. Hayakawa, Phys. Rev. E **58**, 643 (1998).
[8] E. H. Brandt, R. G. Mints, and I. B. Snapiro, Phys. Rev. Lett. **76**, 827 (1996).
[9] S. Gordeev, A. Zhukov, P. de Groot, A. Jansen, R. Gagnon, and L. Taillefer, Phys. Rev. Lett. **85**, 4594 (2000).
[10] M. Rodriguez, G.-S. Paraoanu, and P. Torma, Phys. Rev. Lett. **87**, 100402 (2001).
[11] P. G. de Gennes and J. Prost, *The Physics of Liquid Crystals* (Clarendon Press, Oxford, 1993), 2nd ed., p. 171.
[12] T. E. F. J. D. Bunning and P. L. Sherrel, J. Phys. (Paris) **42**, 1175 (1991).
[13] K. Skarp, S. Lagerwall, and B. Stebler, Mol. Cryst. Liq. Cryst. **60**, 215 (1980).
[14] M. Nobili, C. Lazzeri, A. Schirone, and S. Faetti, Mol. Cryst. Liq. Cryst. **212**, 97 (1992).
[15] G. Tóth, C. Denniston, and J. Yeomans, Phys. Rev. Lett. **88**, 105504 (2002).